Atmos. Chem. Phys. Discuss., 12, 23975–24009, 2012
www.atmos-chem-phys-discuss.net/12/23975/2012/
doi:10.5194/acpd-12-23975-2012

Atmospheric Chemistry and Physics Discussions

Formulation and test of an ice aggregation scheme for two-moment bulk microphysics schemes

E. Kienast-Sjögren[1], **P. Spichtinger**[2], **and K. Gierens**[3]

[1]Institute for Atmospheric and Climate Science, ETH Zurich, Switzerland
[2]Institute for Atmospheric Physics, Johannes Gutenberg-University Mainz, Germany
[3]Deutsches Zentrum für Luft- und Raumfahrt, Institut für Physik der Atmosphäre, Oberpfaffenhofen, Germany

Received: 24 July 2012 – Accepted: 24 August 2012 – Published: 13 September 2012

Correspondence to: E. Kienast-Sjögren (erika.kienast@env.ethz.ch)

Published by Copernicus Publications on behalf of the European Geosciences Union.

Abstract

A simple formulation of aggregation for 2-moment bulk microphysical models is derived. The solution involves the evaluation of a double integral of the collection kernel weighted with the crystal size (or mass) distribution. This quantity is to be inserted into the differential equation for the crystal number concentration which has classical form. The double integrals are evaluated numerically for log-normal size distributions over a large range of geometric mean masses. A polynomial fit of the results is given that yields good accuracy. Various tests of the new parameterization are described: aggregation as stand-alone process, in a box-model, and in 2-D simulations of a cirrostratus cloud. These tests suggest that aggregation can become important for warm cirrus, leading even to higher and longer-lasting in-cloud supersaturation. Cold cirrus clouds are hardly affected by aggregation. The collection efficiency is taken from a parameterization that assumes a dependence on temperature, a situation that might be improved when reliable measurements from cloud chambers suggests the necessary constraints for the choice of this parameter.

1 Introduction

Cirrus clouds, in particular at temperatures higher than −40 °C, often contain very large ice crystals with maximum dimensions exceeding 1 mm (Heymsfield and McFarquhar, 2002, Fig. 4.6). These large crystals generally have complex shapes (Field and Heymsfield, 2003, Fig. 3), and many of them seem to be aggregates of simpler crystals, although one has to be careful in identifying irregular crystals with aggregates (Bailey and Hallett, 2009). Field and Heymsfield (2003) believe that size distributions of ice crystals are dominated by depositional growth for small particles (e.g. up to 100 µm) and dominated by aggregation for larger particles which they underpin by demonstrating that the crystal size distributions for large crystals display a scaling behaviour. “Scaling” is a modern expression for the attainment of a self-preserving size distribution (SPD) (see

ACPD
12, 23975–24009, 2012

Pruppacher and Klett, 1997, ch. 11.7.2, see also Sect. 4.6): The SPD theory suggests that the process of coagulation makes a crystal population loose memory of its inital size distribution and attaining asymptotically a size distribution of a relatively simple form. The further evolution of the latter with time can be described simply by scaling transformations, that is, when the x (size) and y (number) axes are transformed with two simple functions of time ($x'(t) = x\,f_x(t)$, $y'(t) = y\,f_y(t)$), the size distribution is represented by a constant curve in this changing coordinate system. Such scaling behaviour in ice clouds has been demonstrated by several researchers and traced back to a dominance of aggregation processes (e.g. Westbrook et al., 2007).

Although details are unknown it is clear that aggregation can only occur when ice crystals collide. Collisions can be caused by a variety of processes, for instance turbulent motions and gravitational settling of crystals. For crystals larger than a few µm gravitational settling is the most efficient aggregation process (Jacobson, 2005, Fig. 15.7). Turbulent fluctuations in clouds can however enhance the gravitational aggregation process as a result of synergy between dynamics and microphysics (Sölch and Kärcher, 2011): cirrus clouds developing in a steady uplift situation have a thin nucleation zone at their top. New crystals form there as soon as the ongoing cooling drives the relative humidity over the nucleation threshold. The number of new ice crystals is a strong function of $\mathrm{d}S_i/\mathrm{d}t$, the rate at which the supersaturation increases at the threshold. Turbulent motions lead to variations in $\mathrm{d}S_i/\mathrm{d}t$, thus, in consequence, to variations in the number concentration of new crystals. If $\mathrm{d}S_i/\mathrm{d}t$ is by chance particularly low, only few crystals form and they grow subsequently in highly supersaturated air with only weak competition for the excess water vapour. Thus they first grow large by deposition, obtain large fall speeds, and can then collect many ice crystals on their way from cloud top to base.

The dominance of gravitational collection has some consequences: (i) the importance of aggregation decreases with altitude (thus with decreasing temperature) because the absolute humidity decreases (roughly exponentially) and therefore mean crystal dimensions decrease with altitude; (ii) aggregation is more important in deep

ACPD
12, 23975–24009, 2012

than in shallow (ice) clouds; (iii) aggregation is more important in well developed than in young (ice) clouds.

The bulk ice microphysics scheme by Spichtinger and Gierens (2009a) so far did not represent ice aggregation; as only cold cirrus clouds have been simulated, this was tolerable. However, as seen above, aggregation can be an important process and a complete cirrus microphysics scheme must have a representation of it. This new treatment is described in this study. It has to be noted that although the scheme can treat multiple classes of ice (e.g. ice formed by homogeneous nucleation and ice formed by heterogeneous nucleation), it is not yet possible to compute aggregation between these different classes. Therefore we describe here aggregation between crystals of a single class of ice.

2 Mathematical formulation of aggregation for two-moment bulk microphysics schemes

Bulk microphysics schemes do not explicitly resolve the size spectrum of the modelled hydrometeors as spectral models (also known as bin models) or even models following single particles do. Instead, bulk models use only some low order moments of the a-priori assumed size distribution and predict their temporal evolution subject to microphysical processes as nucleation, depositional or condensational growth (and evaporation or sublimation), sedimentation, and aggregation. All these processes can be formulated by first considering the process for a single particle (or two particles in the case of aggregation) and then computing integrals over the assumed size distribution. Two-moment schemes consider the evolution of the zeroth and another low-order moment, which are proportional to the particle number concentration (N) and mass concentration (IWC). If we use particle mass as the quantity characterising particle size, the other moment is of course the first one. If we use instead a linear dimension (e.g. diameter), we have to compute a third moment (in the case of spherical particles) or a more general one (order between 1 and 3) for non-spherical particles like

ACPD
12, 23975–24009, 2012

ice crystals. In the following we present the theory for an assumed mass distribution, which we use in two versions, namely $n(m)\mathrm{d}m$ is the number concentration of particles having masses between m and $m+\mathrm{d}m$, and $f(m)\mathrm{d}m$ is the normalised version of this, namely $f(m) = n(m)/N$ where $N = \int n(m)\mathrm{d}m$ (the total number concentration irrespective of particle mass). This implies $\int f(m)\mathrm{d}m = 1$.

Evidently, aggregation does not change the mass concentration, thus the prognostic equation for IWC is simply

$$\left(\frac{\partial \mathrm{IWC}}{\partial t}\right)_{\mathrm{agg}} = 0.$$

As this paper deals with aggregation alone, we will drop in the following the lower index referring to the process. In order to formulate the differential equation for N we start by writing down the following master-equation (e.g. Pruppacher and Klett, 1997):

$$\frac{\partial n(m,t)}{\partial t} = \frac{1}{2}\int_0^m K(m', m-m')\, n(m',t)\, n(m-m',t)\,\mathrm{d}m' - \int_0^\infty K(m,m')\, n(m,t)\, n(m',t)\,\mathrm{d}m'. \quad (1)$$

Here, $K(m,m')$ is the so-called coagulation kernel (i.e. the rate, at which crystals of mass m coagulate with crystals of mass m') per unit volume. The first rhs integral describes the formation of particles of mass m from aggregation of two smaller particles, and the second rhs integral describes the aggregation of particles of mass m with other crystals of arbitrary mass, which leads to a loss of particles of mass m. Note, that we can extend the 1st integral upper limit to infinity without changing its value because $n(m-m')$ is zero for negative arguments. This fact will be used below.

ACPD
12, 23975–24009, 2012

As stated above, in order to find the prognostic equation for N we have to integrate, i.e.

$$\frac{\partial N(t)}{\partial t} = \frac{\partial}{\partial t}\int_0^\infty n(m,t)\mathrm{d}m = \int_0^\infty \frac{\partial n(m,t)}{\partial t}\mathrm{d}m$$

$$= \frac{1}{2}\int_0^\infty \int_0^\infty \mathrm{d}m\,\mathrm{d}m' K(m',m-m')\,n(m',t)\,n(m-m',t) - \int_0^\infty \int_0^\infty \mathrm{d}m\,\mathrm{d}m' K(m,m')\,n(m,t)\,n(m',t). \quad (2)$$

It is easy to see that every combination of m and m' in the first integral occurs as well in the second one. Thus, both integrals are equal, apart from the factor $1/2$, so that the result is

$$\frac{\partial N(t)}{\partial t} = -\frac{1}{2}\int_0^\infty \int_0^\infty K(m,m')\,n(m,t)\,n(m',t)\,\mathrm{d}m'\,\mathrm{d}m. \quad (3)$$

The derivation of this result is as follows: first we interchange the order of integration in the first integral (I_1), giving

$$I_1 = \int_0^\infty \mathrm{d}m'\,n(m',t)\int_0^\infty \mathrm{d}m K(m',m-m')\,n(m-m',t).$$

Now we substitute x for $m-m'$ in the inner integral, with $\mathrm{d}x = \mathrm{d}m$. The integral limits can still be set to zero and infinity, because n vanishes for negative arguments. Therefore:

$$I_1 = \int_0^\infty \mathrm{d}m'\,n(m',t)\int_0^\infty \mathrm{d}x K(m',x)\,n(x,t).$$

ACPD
12, 23975–24009, 2012

Since it does not matter whether we write the integration variable as x or as m and because the integrand is symmetric in its two variables, we see that I_1 equals the second integral from above, and this completes our proof of Eq. (3).

Now we go on using the normalised mass distribution. In this form, Eq. (3) reads

$$\frac{\partial N(t)}{\partial t} = -\frac{1}{2}N^2 \int_0^\infty \int K(m,m')\, f(m,t)\, f(m',t)\, \mathrm{d}m'\, \mathrm{d}m. \tag{4}$$

In a mathematical sense, the double integral over the kernel function is nothing else than its expectation value for the given distribution $f(m,t)$. This is usually notated as $\langle K \rangle(t)$ where we have retained the time dependence for clarity. The prognostic equation for $N(t)$ is therefore:

$$\frac{\partial N(t)}{\partial t} = -\frac{N(t)^2}{2}\langle K \rangle(t) \tag{5}$$

Assuming that $\langle K \rangle(t)$ is a constant during a single time step Δt in the bulk scheme, there is a formal analytical solution of the form

$$N(t+\Delta t) = \frac{N(t)}{(1/2)N(t)\langle K \rangle(t^*)\Delta t + 1} \tag{6}$$

where t^* is any appropriate time within the time step. The form of this solution has already been obtained by Smoluchowski (1916, 1917) for Brownian coagulation (see also Pruppacher and Klett, 1997, Sect. 11.5). It is seen that for long timesteps such that $\Delta t \gg 1/[N(t)\langle K \rangle(t^*)]$ the final $N(t+\Delta t)$ becomes independent of the initial $N(t)$. With the new value of N and the (here unchanged) value of m we can compute the updated mean mass of $f(m, t+\Delta t)$, i.e. we can compute the updated mass distribution.

The prognostic equation for N is the desired result, and the solution can in principle be computed for arbitrary forms of the mass distribution and for arbitrary coagulation

ACPD
12, 23975–24009, 2012

kernels. Nevertheless, the necessary integrations are tedious and it may be justified to construct a look-up table where the required values of $\langle K \rangle(t)$ can be read off. The computation of the integrals for special choices of $f(m)$ and the kernel is demonstrated next.

3 Computation of the double integrals

3.1 Choice of a mass distribution

In principle we could use any probability density function on $\mathbf{R}^+$ for $f(m)$. Following Spichtinger and Gierens (2009a) we use here a log-normal distribution, i.e.

$$f(m) = \frac{1}{\sqrt{2\pi}\log\sigma_m} \exp\left[-\frac{1}{2}\left(\frac{\log(m/m_m)}{\log\sigma_m}\right)^2\right]\frac{1}{\mathrm{m}} \tag{7}$$

Here, log denotes natural logarithm. The normalized $f(m)$ has two parameters, the modal mass (or geometric mean) m_m which is updated after every time step and the geometric standard deviation σ_m which is usually fixed or formulated as a function of the mean mass.

3.2 Choice of an aggregation kernel

We assume that ice crystals aggregate in particular when large crystals fall through an ensemble of small crystals, when they collide and stick together. This particular mechanism is called gravitational collection and can be described by the following form of a collection kernel (Pruppacher and Klett, 1997, p. 569):

$$K(R,r) := \pi(R+r)^2 |v(R) - v(r)| E(R,r). \tag{8}$$

Here, R and r are the "radii" (see below) of the larger and smaller colliding ice crystals, respectively, such that the first factor on the rhs is the geometric cross section for

ACPD
12, 23975–24009, 2012

the collision. The second factor is the absolute difference of the fallspeeds of the two crystals, that is, the speed of their relative motion. Because of hydrodynamic (and potentially further) effects it is not just the geometric cross section that determines whether two crystals collide, and even if they collide they do not need to stick together. Therefore a correction factor $E(R,r)$ is applied which accounts for these effects. E is usually called collision or collection efficiency. Choices of E will be presented below.

The next problem to solve is to formulate the collection kernel for non-spherical ice crystals instead of spheres. Here we do this for hexagonal cylinders, a common shape for ice crystals as used for instance in Spichtinger and Gierens (2009a). For convenience, the size is replaced by the particle mass. This can be done since mass (m) and size (L) are related (see e.g. Heymsfield and Iaquinta, 2000), usually expressed via power laws (e.g. $m = \alpha L^{\beta}$). Using these relations, we obtain the following expression for the surface of a hexagonal ice crystal of mass m:

$$A(m) = \frac{2}{\rho_\mathrm{b}} \cdot \alpha^{\frac{1}{\beta}} m^{\frac{\beta-1}{\beta}} + 6 \cdot \frac{1}{\alpha^{\frac{1}{\beta}}} \sqrt{\frac{2\alpha^{\frac{1}{\beta}}}{3\sqrt{3}\rho_\mathrm{b}} \cdot m^{\frac{\beta+1}{2\beta}}} \tag{9}$$

where ρ_b = bulk density of ice = $0.81 \times 10^3\,\mathrm{kg\,m^{-3}}$.
Assuming randomly oriented columns (analogous to the usual approximation for radiation parameterization in Ebert and Curry, 1992) we obtain $r^2 = \frac{A(m)}{4\pi}$, such that

$$(R+r)^2 = \frac{1}{4\pi}\left(2\sqrt{A(M)A(m)} + A(M) + A(m)\right) \tag{10}$$

We replace the radii (R,r) with the corresponding masses (M,m) and obtain:

$$K(M,m) = \frac{1}{4}\left(2\sqrt{A(M)A(m)} + A(M) + A(m)\right) \cdot |v(M) - v(m)| E(M,m). \tag{11}$$

The terminal velocity of each of the falling particles can be described using the following power law:

$$v(m) = \gamma m^{\delta} \tag{12}$$

ACPD
12, 23975–24009, 2012

The parameters α, β, γ and δ needed to translate $K(R,r)$ into $K(M,m)$ are given in Spichtinger and Gierens (2009a). Note that the parameters usually are constants for values of m in a certain mass interval. Thus, this leads to a generic splitting of the integrals, as can be seen in the next section.

3.3 Computation of the integrals

The integral values ($\langle K \rangle$ in $\mathrm{m^3\,s^{-1}}$) were calculated using an adaptive Simpson quadrature (e.g. Lyness, 1969) for different values of the geometrical standard deviation σ_m. The calculated integral results for $\sigma_m = 2.85$ are indicated as asterisks in Fig. 1. For reasons given below we compute the integrals with a collision efficiency of unity. The integration was conducted up to a modal mass of 10^6 ng $= 10^{-6}$ kg as this is the upper limit for an aggregated particle, which will be used in the later parameterization. The calculated integral values were divided into four ranges because of mass dependent coefficients α, β, γ and δ. For each range a polynomial was fitted through the calculated values. These polynomials are displayed as solid lines in Fig. 1. The four polynomial ranges correspond to changes in the growth and sedimentation behaviour of ice crystals (e.g. changes of the parameters $\alpha, \ldots, \delta$) as indicated in Spichtinger and Gierens (2009a):

1. 1×10^{-4} ng $< m_m \leq 2.5\times10^{-3}$ ng: mainly hexagonal ice crystals with aspect ratio 1.
2. 2.5×10^{-3} ng $< m_m \leq 4 \times 10^{2}$ ng: columns with aspect ratio larger than 1.
3. 4×10^{2} ng $< m_m \leq 1 \times 10^{4}$ ng: the sedimentation velocity gets larger.
4. 1×10^{4} ng $< m_m$: even larger columns.

As can be seen in Fig. 1, the polynomial fits to the exact integral values are very good; the maximum deviation is less than 10 % and the mean deviation even less than 2 %. Thus the polynomials can be used as an accurate solution while saving computing time.

ACPD
12, 23975–24009, 2012

4 Various tests

The change in particle number density per timestep is described in (5) as:

$$\frac{\partial N(t)}{\partial t} = -\frac{N(t)^2}{2}\langle K\rangle(t)$$

The solution of this can either be achieved through an exact solution involving separation of variables with the following result:

$$N(t+\Delta t) = \frac{N(t)}{(1/2)N(t)\langle K\rangle(t^*)\Delta t + 1} \tag{13}$$

or through the following Euler approximation:

$$N(t+\Delta t) = N(t) + \frac{\partial N(t)}{\partial t}\cdot\Delta t = N(t) - \frac{N(t)^2}{2}\langle K\rangle(t)\cdot\Delta t \tag{14}$$

Tests have shown that both methods give practically identical results. The following tests have been performed with the Euler approximation. Further tests have shown that the polynomial approximation of the $\langle K\rangle$ integrals was a sufficient approximation (see above), so the following tests have been performed using the polynomial approximation.

4.1 Test of aggregation only

4.1.1 Maximum aggregation

The new formulation of the aggregation process was tested in MATLAB with different start values for the particle number density ranging from 10 to 5×10^3 particles per litre. We let aggregation occur as the only process. We set $E \equiv 1$ for these tests, that is, the following results show a maximum effect of aggregation. The aggregation was run for

ACPD
12, 23975–24009, 2012

1000 s, i.e. approximately 17 min. If aggregation occurs, the particle number density N will decrease. The modal mass will increase in turn and the new $f(m)$ is used in the next timestep. For the calculations, we set an upper boundary for the mass of the aggregated particles at 10^{-6} kg, which corresponds to a particle size of 8 mm. Larger ice crystals will not occur in the model.

Figure 2 shows the results of these tests. For small initial modal masses (e.g. 10^{-11} kg, green line) and starting with, for example, 10^5 particles m^{-3}, after simulating 1000 s we still have 10^5 particles m^{-3}. Thus almost no aggregation occurs. If the initial modal mass is instead increased to 10^{-9} kg (blue line) while still starting with 10^5 m^{-3} particles, we only have about 10^4 m^{-3} particles left after 1000 s. Thus about 90 % of the particles have aggregated.

As expected, when small crystals (i.e. small modal masses) predominate, nothing happens. The probability for collision is negligible and the relative fall speeds are low. The larger the particles get, the more they aggregate. For the largest initial modal masses (i.e. 10^{-9} kg) the particles stick together very fast so that the iteration has to be stopped before reaching 1000 s.

Timesteps from 0.1 s (timescale for microphysics) to 10 s (timescale for dynamics) gave very similar results, that is, the parameterization is consistent with different timesteps. We chose to use a timestep of 1 s.

4.1.2 Introducing temperature dependency

Experience from field measurements suggests that aggregation occurs more efficiently in warmer than in colder air (e.g. Kajikawa and Heymsfield, 1989). This experience is expressed by the following parameterization for the collision efficiency of ice crystals (Lin et al., 1983; Levkov et al., 1992) which is independent of the crystal masses and dependent only on temperature:

$$E(T) = \exp(0.025 \cdot (T - 273.16)) \quad (15)$$

ACPD
12, 23975–24009, 2012

With this parameterization, E can be taken out from the integral calculation and treated as a prefactor.

The temperature dependent collision efficiency is $E \ll 1$ for typical temperatures in ice clouds. Thus we expect strongly reduced aggregation effects on N compared to the previous tests when we introduce the new factor. Figure 3 shows the final crystal concentrations as before for aggregation without temperature dependency ($E = 1$) and for different temperatures. As expected, with decreasing temperature aggregation becomes less important. Even at the highest considered temperature (240 K) the reduction of the aggregation effect is considerable, in particular for high initial number densities. This finding is a good argument for ignoring aggregation in simulations of cold cirrus clouds where not only E is small but also the median crystal masses are smaller than in warm cirrus.

4.2 Test of aggregation within a box model

The following tests have been performed assuming a temperature dependent efficiency $E(T)$ in order to see a realistic impact of aggregation on cirrus clouds.

4.2.1 Model description and setup

In this section we test the effect of aggregation on the ice crystal number concentration in the framework of a box model (Spichtinger and Gierens, 2009a) which we consider a more realistic test in that various microphysical processes can act simultaneously. The box is thought to represent an initially cloud free air parcel which is lifted with a constant vertical velocity. The displayed results are calculated with $w = 0.05\,\mathrm{m\,s^{-1}}$. We choose initial temperatures of 210 K and 240 K in order to obtain results with a small collision efficiency (cold) and a moderately large one (warm). The box starts to rise at an initial pressure of 300 hPa. Apart from homogeneous nucleation and depositional ice crystal growth, the process of sedimentation is treated in the box model as described in Spichtinger and Cziczo (2010). From the ice mass concentration (IWC) and the

ACPD
12, 23975–24009, 2012

mass-mean terminal velocity of the ice crystals an ice mass flux density $F = \mathrm{IWC}\,\overline{v_m}$ is computed for the box with

$$\overline{v_m} = \frac{1}{\mathrm{IWC}} \int f(m) \cdot m \cdot v(m)\,\mathrm{d}m. \tag{16}$$

We assume then that the ice mass flux density at the bottom of the box is $F_{\mathrm{bottom}} = F$. A sedimentation parameter f_{sed} is introduced to determine the sedimentation flux density into the top of the box:

$$F_{\mathrm{top}} = f_{\mathrm{sed}} F_{\mathrm{bottom}}, \tag{17}$$

whereby it is possible to categorise different sedimentation scenarios:

- $f_{\mathrm{sed}} = 1.0$ corresponds to no sedimentation as net effect. The flux exiting the lower part of the box has the same magnitude as the flux entering the top of the box.
- $f_{\mathrm{sed}} = 0.9$ corresponds to regions in the middle and lower part of the cloud. The flux leaving the region is almost but not completely balanced by the flux entering that region from above.
- $f_{\mathrm{sed}} = 0.5$ corresponds to the top region of a cloud. The flux leaving that region is only half balanced by a flux from above.

4.2.2 Results for an initial temperature of 240 K

As a baseline experiment we consider first a case without the effect of sedimentation, that is, with $f_{\mathrm{sed}} = 1$. The temporal variation of the crystal number density in the box is shown in Fig. 4. As the box is cooled down from 240 K, the threshold supersaturation for homogeneous nucleation is reached about 120 min later, and the nucleation burst leads to a high crystal concentration ($\approx 2 \times 10^4$ m^{-3}). The further development depends strongly on whether we include aggregation or not. Without aggregation, the

ACPD
12, 23975–24009, 2012

crystal concentration stays essentially constant (a weak reduction is caused by the expansion of the lifting box). With aggregation, however, the crystal concentration decreases strongly (by about 90 %) within two hours. This happens in this academic case because the large crystals effectively stay within the box (the crystals leaving the box are replaced by identical crystals entering from above) and aggregate over the whole simulation time.

Now we turn sedimentation on, allowing the large crystals to leave the box without complete replacement from above. For the top region of the clouds ($f_{sed} = 0.5$), the results are displayed in Fig. 5. Again, nucleation occurs after 120 min and a large number of ice crystals appears. These grow by vapour deposition and RH_i decreases. Sedimentation is a much more important process now than aggregation, which can be seen from the time scale of the decrease of N which occurs much faster than in the previous case where sedimentation was switched off. The two curves representing the cases with and without aggregation are almost identical up to 200 min when a second nucleation burst occurs. This is possible because RH_i starts to increase again because of the ongoing cooling when N is sufficiently diminished. As aggregation contributes to the reduction of N (albeit much less effective than sedimentation) the second nucleation burst occurs slightly earlier (a few minutes) in the case with aggregation than in the other case.

In the middle of the cloud, where a good deal of falling ice crystals are replaced by crystals falling from above ($f_{sed} = 0.9$), aggregation is a bit more important than at the top of the cloud. This is shown in Fig. 6. We see that the reduction of N after the nucleation burst is slower than at the top of the cloud because more falling crystals are replaced. Aggregation accelerates the reduction of N such that a certain level of N is now reached some ten minutes earlier in the case with aggregation than without. A second nucleation burst does not occur in either case in the middle of the cloud until the end of the simulation.

ACPD
12, 23975–24009, 2012

4.2.3 Initial temperature of 210 K

The box model simulations at 240 K have shown that aggregation generally has a weak effect on the evolution of crystal number concentrations. Since the collision efficiency decreases exponentially with decreasing temperature, we therefore expect a negligible effect of aggregation at the low temperature of 210 K, for all choices of f_{sed}. This is indeed what we found from our box model simulations: the curves for the cases with and without aggregation are practically identical, therefore it is not necessary to display them here.

4.3 Test of aggregation within a 2-D model: simulations of synoptically driven cirrostratus

In order to investigate the impact of aggregation in a more realistic situation we implemented the new aggregation parameterization into the EULAG model including the already mentioned bulk microphysics scheme (Spichtinger and Gierens, 2009a). We investigate typical formation conditions for stratiform cirrus clouds, i.e. a synoptic scale updraught. In the next subsection we present the setup of the simulations. Then we will present and discuss the results.

4.4 Setup

For simulating stratiform cirrus clouds as typical for mid latitudes we specify vertical profiles of temperature and pressure as shown in Fig. 7, respectively; additionally, we prescribe an ice-supersaturated layer with vertical extension of $\Delta z = 1.5$ km at different altitudes (top of layer at $z_{top} = 9/10/11$ km, i.e. low/middle/high). The vertical extension and the corresponding temperature ranges are presented in Table 1. We use a 2-D domain (x-z-plane) in the troposphere with a horizontal extension $L_x = 12.7$ km ($\Delta x = 100$ m) and a vertical extension $4 \leq z \leq 14$ km ($\Delta x = 50$ m). At initialisation the potential temperature field is superimposed by Gaussian noise

ACPD
12, 23975–24009, 2012

with standard deviation $\sigma_T = 0.025\,\mathrm{K}$. We choose a moderate wind shear for horizontal wind, i.e. $\mathrm{d}u/\mathrm{d}z = 10^{-3}\,\mathrm{s}^{-1}$ with $u(z=0) = 0\,\mathrm{m\,s}^{-1}$, leading to a maximum wind of $u_{\max} \approx 10\,\mathrm{m\,s}^{-1}$ at $z = 14\,\mathrm{km}$. The whole 2-D domain is lifted with a constant vertical velocity. In order to investigate different synoptic conditions we choose two values $w = 5\,\mathrm{cm\,s}^{-1}$ and $w = 8\,\mathrm{cm\,s}^{-1}$. In order to obtain similar conditions at the end of the simulations (i.e. the same vertical distance of lifting $\Delta z_{\mathrm{lift}} = 720\,\mathrm{m}$ or equivalently a cooling of $\Delta T \approx 7.04\,\mathrm{K}$), the simulation time is adjusted; in case of $w = 5\,\mathrm{cm\,s}^{-1}$ the total simulation time is $\Delta t = 240\,\mathrm{min}$, whereas for $w = 8\,\mathrm{cm\,s}^{-1}$ the total simulation time is $\Delta t = 150\,\mathrm{min}$. As the results turned out to be similar for the chosen vertical velocities in terms of impact of aggregation, we will concentrate on a detailed investigation of the case $w = 5\,\mathrm{cm\,s}^{-1}$. For investigating the impact of aggregation we use three different setups: In the reference case, we switch off aggregation; in scenario "temperature-dependent" we use the full aggregation parameterization including the temperature dependency, as described in Sect. 4.1.2. In order to see the maximum effect of aggregation, we use the scenario "maximum impact", i.e. here the aggregation has efficiency $E \equiv 1$. We assume that ice forms by homogeneous nucleation only. The background aerosol (sulphuric acid) is prescribed with a lognormal distribution with (dry) modal radius $r_m = 25\,\mathrm{nm}$ and geometrical standard deviation of $\sigma_r = 1.5$.

4.5 Results and discussion

In general the simulations behave similar to those carried out by Spichtinger and Gierens (2009b) for the case of pure homogeneous nucleation: as the domain is lifted it cools by adiabatic expansion and the relative humidity increases until crystals are formed at the threshold for homogeneous nucleation. Figure 8 shows the temporal evolution of the reference simulation in time steps of 30 min. The formation of a quite homogeneous cirrostratus can be seen to occur after about 2 h simulation time. Some structure is formed by the horizontal wind driving small circulations inside the layer. Figure 9 shows the results at the end of the simulations. Mean values of ice water content,

ACPD
12, 23975–24009, 2012

ice crystal number concentration and relative humidity wrt ice are shown, averaged over the domain. As expected, the impact of aggregation increases with temperature, even in the cases with $E \equiv 1$ where the aggregation efficiency itself has no temperature dependence. Obviously the remaining factors in the collision kernel contribute significantly to the temperature dependence and this is due to the fact that crystals can grow larger in the higher absolute humidity environment at higher temperatures. Thus, the geometrical factor evidently grows with temperature. The factor depending on the difference of terminal fall speeds increases on average with mean crystal size if the width of the size distribution does so. In the formulation of Spichtinger and Gierens (2009a) the width of the mass distribution (i.e. the square root of the second central moment) is proportional to the mean mass. Therefore higher temperatures lead to more aggregation also via the terminal velocities in this model.

Aggregation increases the average mass of ice crystals and so leads to stronger sedimentation which has an effect on ice mass and number concentration in the simulated clouds. Mean crystal number concentrations and ice water contents are strongly (up to and partly exceeding a factor 2) reduced by aggregation in the simulation using the highest temperature. The effects are of similar quality in the colder cases, but smaller. Effects on the mean profiles of relative humidity are present, but here it is more instructive to look at the statistics (see below, Fig. 10). The pdfs of number concentration of ice crystals display in our simulations broad maxima at around $N_i \sim 100\,\mathrm{l}^{-1}$. Whereas there is hardly any effect on the statistics of number concentration in the low temperature case, aggregation shifts the peaks to lower values and broadens them. As expected, this effect becomes more prominent at higher temperatures. This is clearly a signature of the aggregation-enhanced sedimentation (see also discussion in Spichtinger and Gierens, 2009a). The high number concentration tails of the distributions are merely little affected by aggregation; this is quite plausible because high number concentrations are usually coupled with small ice crystals, thus aggregation is weakly effective in this range.

ACPD
12, 23975–24009, 2012

Also the total surface area of the ice crystals decreases by aggregation. This and the above mentioned increase of sedimentation fluxes diminish the sink for supersaturation and higher relative humidities are maintained over longer periods of time compared to the reference cases without aggregation. The statistics of relative humidities typically peak at values slightly above 100 %. This is best seen in the cold case where aggregation has hardly any effect on the pdf of RHi. At the higher temperatures, where aggregation becomes more efficient we see the peaks shifted to higher values (i.e. more significant "quasi equilibrium" supersaturation), clearly an effect of the less effective sink for water vapour in a cloud affected by aggregation (see also the discussion in Spichtinger and Cziczo, 2010). This effect is most pronounced in those regions of a cloud that otherwise approach ice saturation most quickly, typically the middle part of the cloud. Thus aggregation contributes to ice supersaturation within relatively warm cirrus clouds. Cold cirrus is hardly affected by aggregation according to our simulations (and under the condition that the gravitational collection kernel is the only relevant one for cirrus clouds).

In the simulations with stronger updraught we can see differences in details, but qualitatively they behave similar to the simulations shown. Therefore we do not deem it necessary to present them here.

4.6 Scaling size distribution

The log-normal crystal mass distribution is used in the scheme of Spichtinger and Gierens (2009a) and the question arises whether this is an appropriate choice in situations where aggregation dominates ice growth. In such cases the evolving crystal size distribution apparently can be mapped onto a universal shape:

$$f(m,t) = \left(\frac{m_m(t)}{m_0}\right)^{-\theta} \psi\left(\frac{m}{m_m(t)}\right),$$

where m_0 is a mass unit (to make the prefactor dimensionless) and $\psi(x)$ is a function that depends on time only via the ratio $m/m_m(t)$ but not otherwise

ACPD
12, 23975–24009, 2012

(Field and Heymsfield, 2003; Westbrook et al., 2004, 2007; Sölch and Kärcher, 2011). The temporal evolution of the size distribution can thus be captured by scaling both axes with a function of the time-varying modal mass, the m-axis with its inverse and the f-axis with its θ-th power. Although the log-normal distribution can be treated in this way (with $\theta = 1$ for constant geometric width), it is not a true solution for gravitational aggregation. Researchers, guided by numerical simulations, tend to use for $\psi(x)$ functions with an exponential upper tail (e.g. Field and Heymsfield, 2003, use a gamma distribution), however, it is not mathematically proven that the gravitational collection kernel has a scaling solution at all (Aldous, 1999). One condition for this is the homogeneity of the kernel function $K(m, M)$. From the mass-length and length-fall speed relations we can see that the kernel can only be a homogeneous function if the exponents in these relations are constant over all sizes. This is only so for spheres. The exponents change, however, with size for ice crystals and the shape of the crystals, for instance expressed by the aspect ratio, changes with size (see, for instance, Heymsfield and Iaquinta, 2000). In our case with hexagonal columns it is the function $A(m)$, the surface of the crystal, where m appears with two different exponents (for the basal and prism faces, respectively); $A(m)$ is non-homogeneous. Hence, for ice the collection kernel is not a homogeneous function and therefore there is no true scaling. If it is nevertheless possible to match observed size distributions to a universal scaling function, this suggests that there is an approximate scaling for large ($\gg 100\,\mu m$) crystals, which requires that the mentioned exponents are mainly constant in this range. The upper tail of a log-normal distribution is slightly upward on a semilog plot, that is, it has not a perfect exponential shape; but it might be possible to fit the observed size distributions of large crystals with log-normals as well as with gamma-distributions (in particular, given the noise in the data). Unless there is a mathematical proof that ice aggregation leads to a specific size distribution other than the log-normal there is no need to abandon it.

ACPD
12, 23975–24009, 2012

5 Conclusions

We have derived from the master-equation for coagulation a simple formulation of aggregation for 2-moment bulk microphysical models. So far we developed the formulation for aggregation of crystals belonging to the same class only (the microphysics scheme of Spichtinger and Gierens (2009a) allows more than one class of ice). A more general formulation with aggregation of crystals from different classes is rather a numerical than a mathematical problem, but a difficult one, and we have not tried yet to solve it. The core of the present formulation is a double integral of the collection kernel weighted with the crystal size (or mass) distribution, which is the expectation value of the kernel. This quantity is to be inserted into the differential equation for the crystal number concentration which is of a form that was already derived by Smoluchowski (1916, 1917). The double integrals are evaluated numerically for log-normal size distributions over a large range of geometric mean masses. The direct evaluation of the integrals within a cloud simulation run takes a lot of computing time and is not recommended. Instead the pre-calculated results can either be read from a look-up table or – even better – a polynomial fit of the results can be used that yields good accuracy.

We have tested the new parameterization in various environments: stand-alone (to see how the solution of the differential equation behaves and to test the polynomial fits), in a box-model (where aggregation occurs simultaneously with other microphysical processes and where a first check can be made, whether and when it is important), and in a 2-D simulation of a cirrostratus cloud (where additionally cloud dynamics can enhance or dampen the effects of aggregation). Overall these tests suggest that aggregation can become important at (relatively) warmer cirrus temperatures, affecting not only ice number and mass concentrations, but leading also to higher and longer-lasting in-cloud supersaturation. Sedimentation fluxes are increased when aggregation is switched on. Cold cirrus clouds are hardly affected by aggregation. The temperature dependence originates not only from an assumed temperature dependence of the collection efficiency but also from the other factors in the collision kernel: higher

ACPD
12, 23975–24009, 2012

temperatures imply larger ice crystals and larger spread in terminal velocities (if the assumed type of size distribution is such, that the width of it increases with increasing mean size). For cold clouds it is often justified to ignore aggregation when the research focus is on ice mass and number densities. However, when the focus of research is crystal habits and their effect on radiation, aggregation should not be ignored since cirrus clouds usually contain complex, irregular and imperfect ice crystals as reported by Bailey and Hallett (2009). The authors have shown that even cold cirrus contains complex ice crystals that may be the result of aggregation. They occur predominantly at high supersaturation, but supersaturation does not directly appear in the formulation of the kernel function. One might test whether an extension of the formulation of the collection efficiency (i.e. $E = E(T, S)$) yields better results, but there is much freedom for playing. Rather it is desirable to measure collection efficiencies in big cloud chambers. By doing so, one should simultaneously test whether aggregation is the only process that leads to complex forms of ice crystals. This is not probable since rosette shaped crystals are too regular to be formed by random collisions. There is obviously a gap in our understanding and much occasion remains for further experimental research before we should develop our numerical formulations into unjustified detail.

Acknowledgements. KG contributes with the model improvement to the DLR project CATS. The numerical simulations with the 2-D model were carried out at the European Centre for Medium-Range Weather Forecasts (special project “Ice supersaturation and cirrus clouds”).

References

Aldous, D. J.: Deterministic and stochastic models for coalescence (aggregation and coagulation): a review of the mean-field theory for probabilists, Bernoulli, 5, 3–48, 1999. 23994

Bailey, M. P. and Hallett, J.: A comprehensive habit diagram for atmospheric ice crystals: confirmation from the laboratory, AIRS II, and other field studies, J. Atmos. Sci., 66, 2888–2899, 2009. 23976, 23996

Ebert E. and Curry J.: A parameterization of ice cloud optical properties for climate models, J. Geophys. Res., 97, 3831–3836, 1992. 23983

ACPD

12, 23975–24009, 2012

Field, P. R. and Heymsfield, A. J.: Aggregation and scaling of ice crystal size distributions, J. Atmos. Sci., 60, 544–560, 2003. 23976, 23994
Heymsfield, A. and Iaquinta, J.: Cirrus crystal terminal velocities, J. Atmos. Sci., 57, 916–938, 2000. 23983, 23994
Heymsfield, A. J. and McFarquhar, G. M.: Mid – latitude and tropical cirrus, in: D. K. Lynch, K. Sassen, D. O' C. Starr, and G. Stephens (Eds.): Cirrus, Oxford Univ. Press, New York (USA), 78–101, 2002. 23976
Jacobson, M. Z.: Fundamentals of Atmospheric Modeling, 2nd Ed., Cambridge Univ. Press, Cambridge (UK), xiv and 813 pp., 2005. 23977
Kajikawa, M. and Heymsfield, A.: Aggregation of ice crystals, J. Atmos. Sci., 46, 3108–3121, 1989. 23986
Lin, Y., Farley, R. D. and Orville, H. D.: Bulk parameterization of the snow field in a cloud model, J. Appl. Meteorol., 22, 1065–1092, 1983. 23986
Levkov, L., Rockel, B., Kapitza, H. and Raschke, E.: 3-D mesoscale numerical studies of cirrus and stratus clouds by their time and space evolution, Contrib. Atmos. Phys., 65, 35–58, 1992. 23986
Lyness, J. N.: Notes on the adaptive simpson quadrature routine, J. ACM, 16, 483–495, doi:10.1145/321526.321537, 1969. 23984
Pruppacher, H. R. and Klett, J. D.: Microphysics of Clouds and Precipitation, Kluwer Academic Publishers, Dordrecht, Holland, 1997. 23977, 23979, 23981, 23982
Smoluchowski, M.: Drei Vorträge über Diffusion, Brownsche Bewegung und Koagulation von Kolloidteilchen, Z. Physik., 17, 557–585, 1916. 23981, 23995
Smoluchowski, M.: Versuch einer mathematischen Theorie der Koagulationskinetik kolloider Lösungen, Z. Phys. Chem., 92, 129–168, 1917. 23981, 23995
Sölch, I., and Kärcher, B.: Process – oriented large – eddy simulations of a midlatitude cirrus cloud system based on observations, Q. J. Roy. Meteor. Soc., 137, 374–395, 2011. 23977, 23994
Spichtinger, P. and Cziczo, D. J.: Impact of heterogeneous ice nuclei on homogeneous freezing events in cirrus clouds, J. Geophys. Res., 115, 14208, doi:10.1029/2009JD012168, 2010. 23987, 23993
Spichtinger, P. and Gierens, K.: Ice supersaturation in the tropopause region over Lindenberg, Germany, Meteorol. Z., 12, 143–156, 2003.

ACPD
12, 23975–24009, 2012

Spichtinger, P. and Gierens, K. M.: Modelling of cirrus clouds – Part 1a: Model description and validation, Atmos. Chem. Phys., 9, 685–706, doi:10.5194/acp-9-685-2009, 2009a. 23978, 23982, 23983, 23984, 23987, 23990, 23992, 23993, 23995

Spichtinger, P. and Gierens, K. M.: Modelling of cirrus clouds – Part 2: Competition of different nucleation mechanisms, Atmos. Chem. Phys., 9, 2319–2334, doi:10.5194/acp-9-2319-2009, 2009b. 23991

Westbrook, C. D., Ball, R. C., Field, P. R., and Heymsfield, A. J.: Theory of growth by differential sedimentation, with application to snowflake formation, Phys. Rev. E, 70, 021403-1–021403-7, 2004. 23994

Westbrook, C. D., Hogan, J. R., Illingworth, A. J., and O'Connor, E. J.: Theory and observations of ice particle evolution in cirrus using Doppler radar: evidence for aggregation, Geophys. Res. Lett., 34, 02824, doi:10.1029/2006GL027863, 2007. 23977, 23994

ACPD

12, 23975–24009, 2012

Table 1. Initial vertical positions and temperature ranges for ice-supersaturated layers (low/middle/high).

Layer	altitude (km)	temperature (K)
low	$7.5 \leq z \leq 9$	$235.3 \geq T \geq 222.3$
middle	$8.5 \leq z \leq 10$	$226.8 \geq T \geq 213.5$
high	$9.5 \leq z \leq 11$	$217.9 \geq T \geq 204.6$

ACPD
12, 23975–24009, 2012

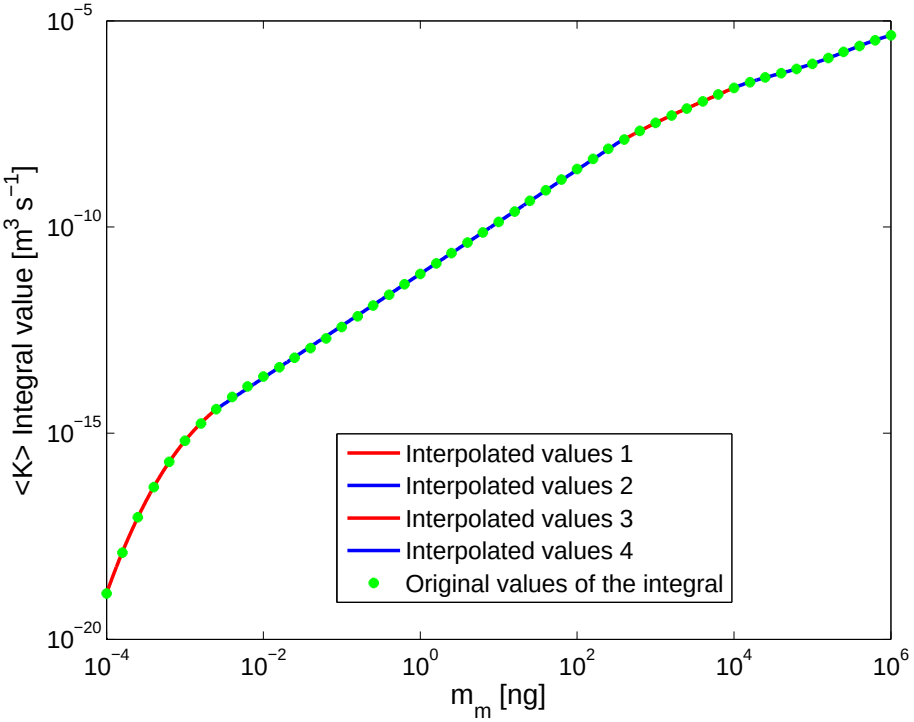

Fig. 1. $\langle K \rangle$ integral values (in $m^3 s^{-1}$) as a function of the geometric mean mass (in ng) of the crystal mass distribution and for $\sigma_m = 2.85$. The corresponding sizes range between a modal length of 0.6 and 8000 µm. Exact values from a numerical integration are shown as asterisks. The solid lines represent polynomial fits in 4 different mass ranges.

ACPD
12, 23975–24009, 2012

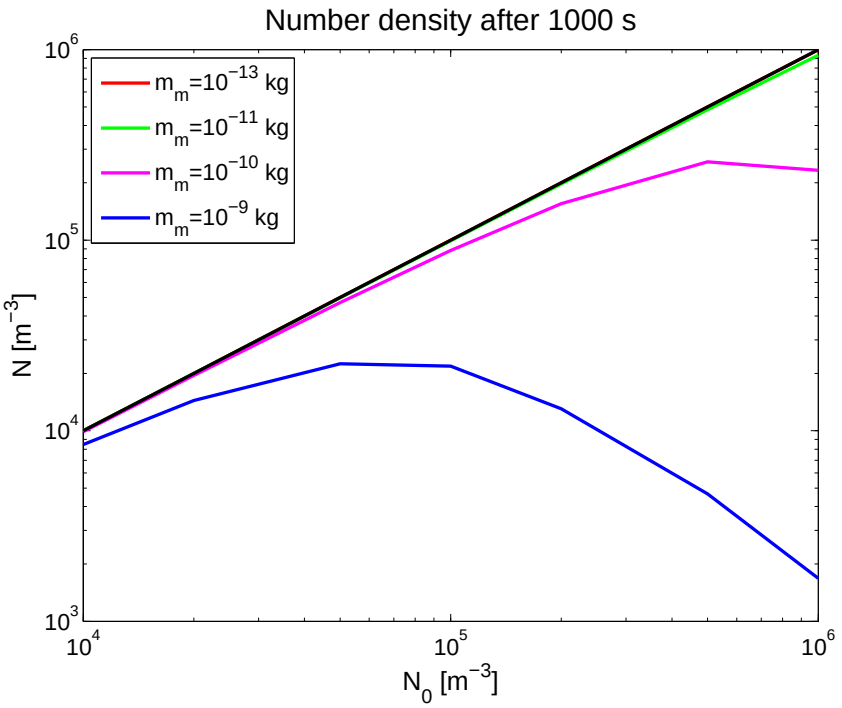

Fig. 2. Particle number density N_0 at the start of the iteration (x-Axis) and after 1000 s of iteration (N, y-Axis). For small modal masses, the particle number density hardly changes during the iteration and the plot is almost a straight line. As reference for no aggregation, a black line is plotted. As expected, larger modal masses result in increased aggregation. Thus the particle number density decreases during integration, which is shown in the graph. The corresponding size to the modal masses plotted ranges between 6 and 345 µm. Note that the tests have been performed with $E \equiv 1$, that is, the maximum effect of aggregation is seen here. The red line is almost equal to the black line, thus can hardly be seen in the plot.

ACPD
12, 23975–24009, 2012

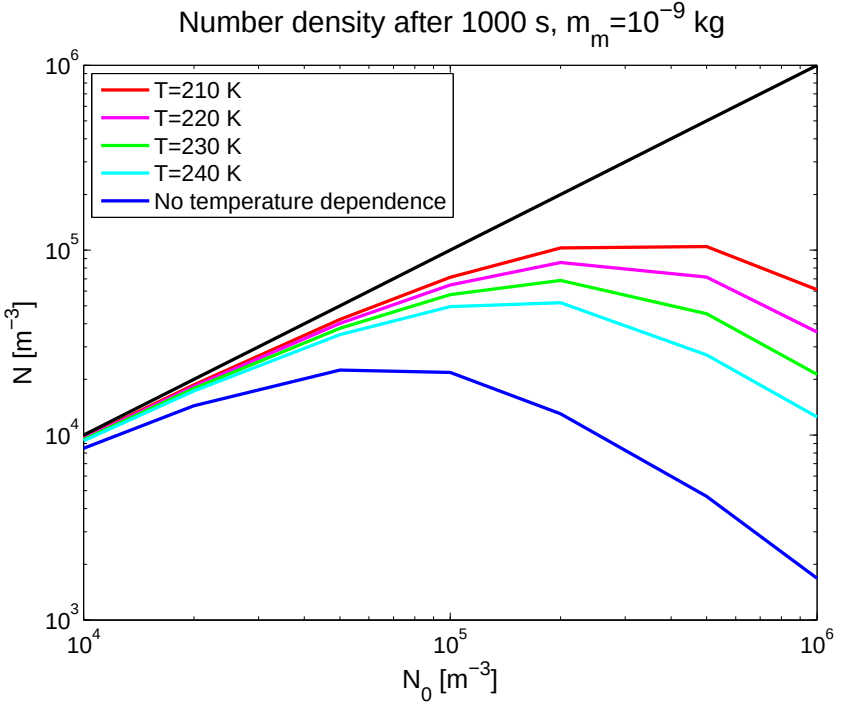

Fig. 3. Particle number density N_0 at the beginning of the iteration (x-Axis) and after 1000 s of iteration (N, y-Axis) for a modal mass of 10^{-9} kg, which corresponds to a particle with modal length 345 µm. As a reference for no aggregation, a black line is plotted. Adding a temperature dependency shows a weakened aggregation effect with decreasing temperatures. The lower the temperatures the more particles are present at the end of the simulation.

ACPD
12, 23975–24009, 2012

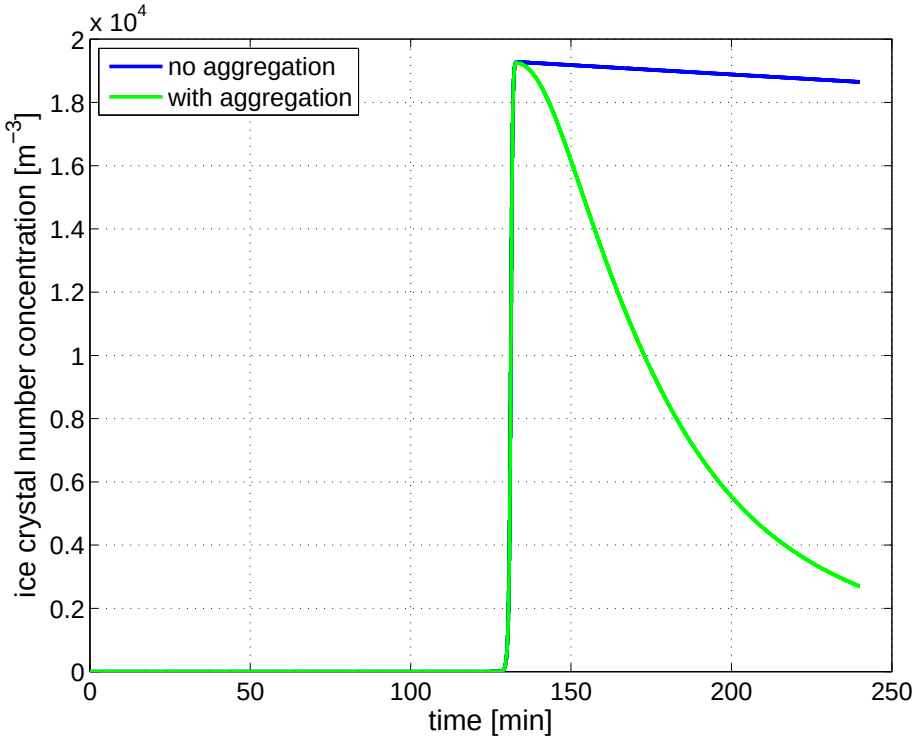

Fig. 4. Ice crystal number concentration as a function of time. Initial temperature is 240 K $f_{sed} = 1.0$. Green line: case with aggregation; blue line: without aggregation. As there is no sedimentation, aggregation is the only sink process.

ACPD
12, 23975–24009, 2012

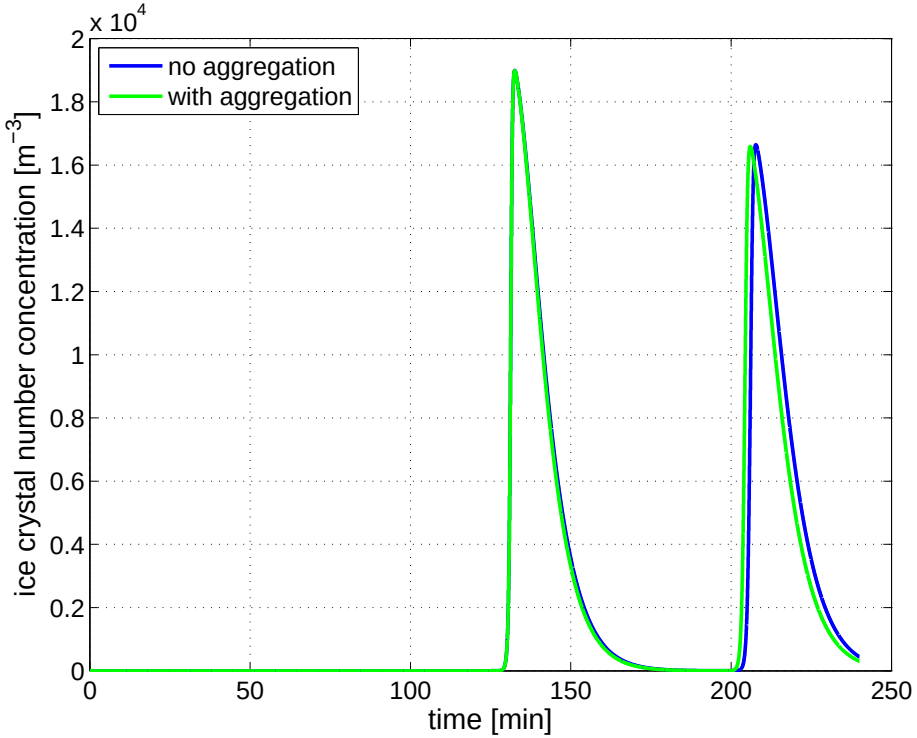

Fig. 5. Same as Fig. 4, but with $f_{sed} = 0.5$, corresponding to the top region of a cloud. Hardly any effect of aggregation is observed after the first nucleation burst. The second nucleation takes place slightly earlier if aggregation is turned on.

ACPD
12, 23975–24009, 2012

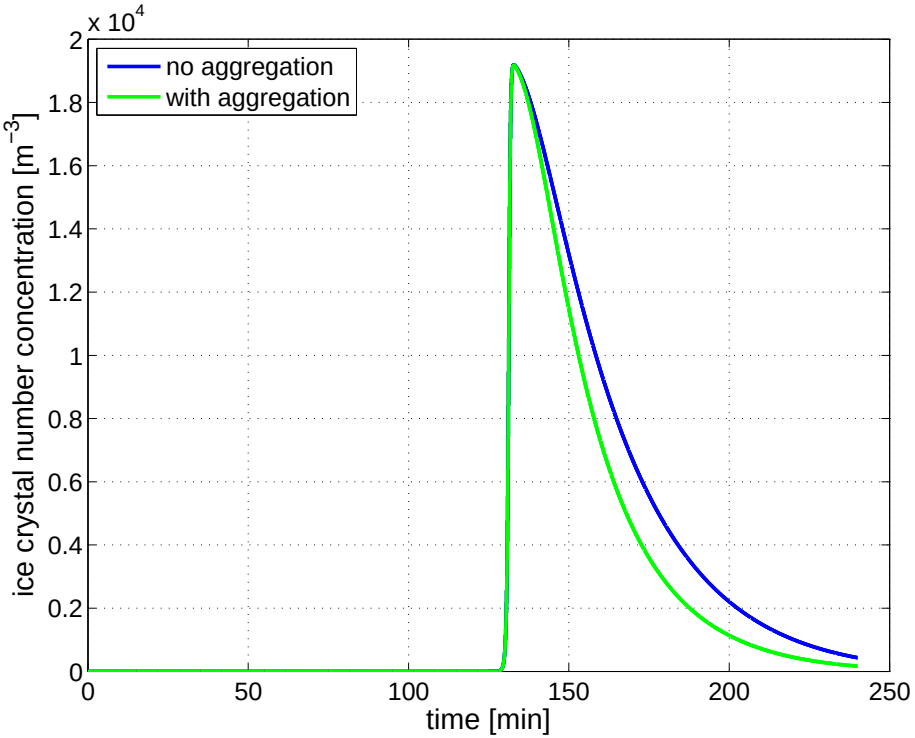

Fig. 6. Same as Fig. 4, but with $f_{sed} = 0.9$, corresponding to the inner region of a cloud. With aggregation, the crystal number density is decreasing slightly faster than with only sedimentation.

ACPD
12, 23975–24009, 2012

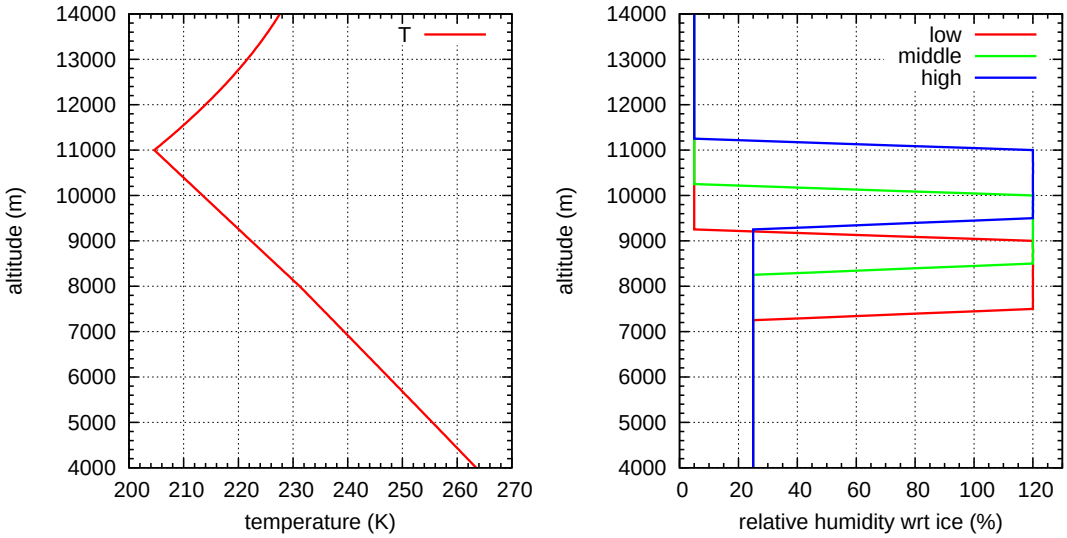

Fig. 7. Initial vertical profiles for the simulations; left: temperature, middle: pressure, right: relative humidity wrt ice for different setups (low, middle and high altitude range, corresponding to high, medium and low temperature range, see Table 1).

ACPD
12, 23975–24009, 2012

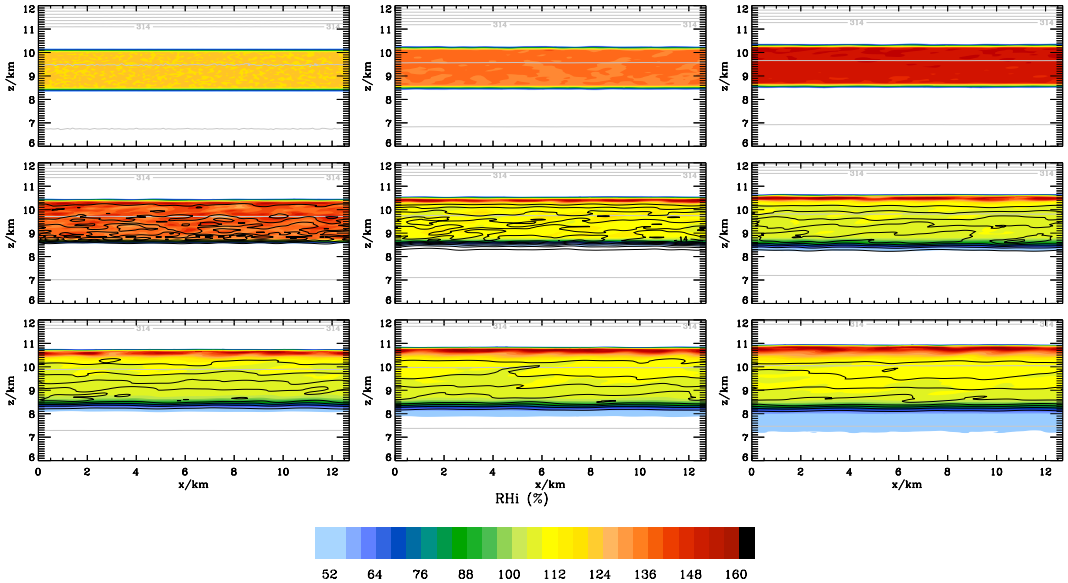

Fig. 8. Time evolution of reference simulation with a time increment of Δt = 30 min (upper row: 0/30/60 min; middle row: 90/120/150 min; lower row: 180/210/240 min). Black isolines indicate ice water content, grey lines indicate isentropes.

ACPD
12, 23975–24009, 2012

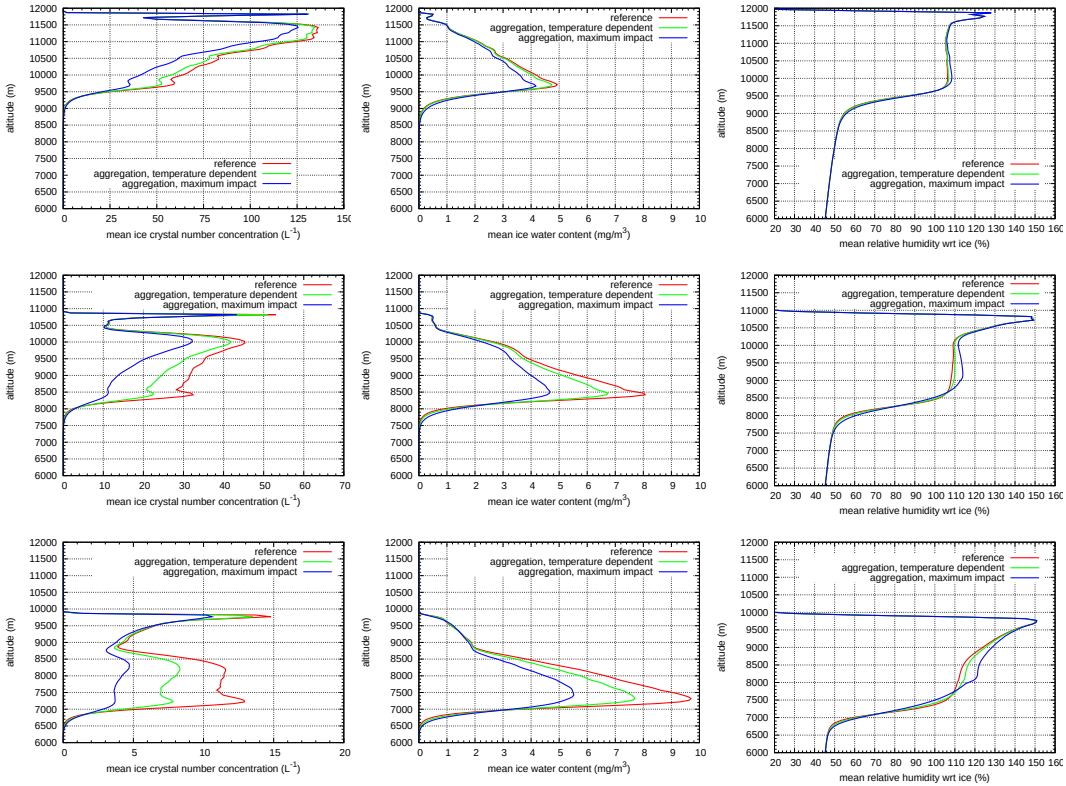

Fig. 9. Vertical profiles of mean ice crystal number concentration (left), ice water content (middle) and relative humidity wrt ice (right) at the end of the simulation (t = 240 min, w = 5 cm s^{-1}) for different temperature regimes. Top row: low temperature conditions, middle row: medium temperature conditions, bottom row: high temperature conditions.

ACPD
12, 23975–24009, 2012

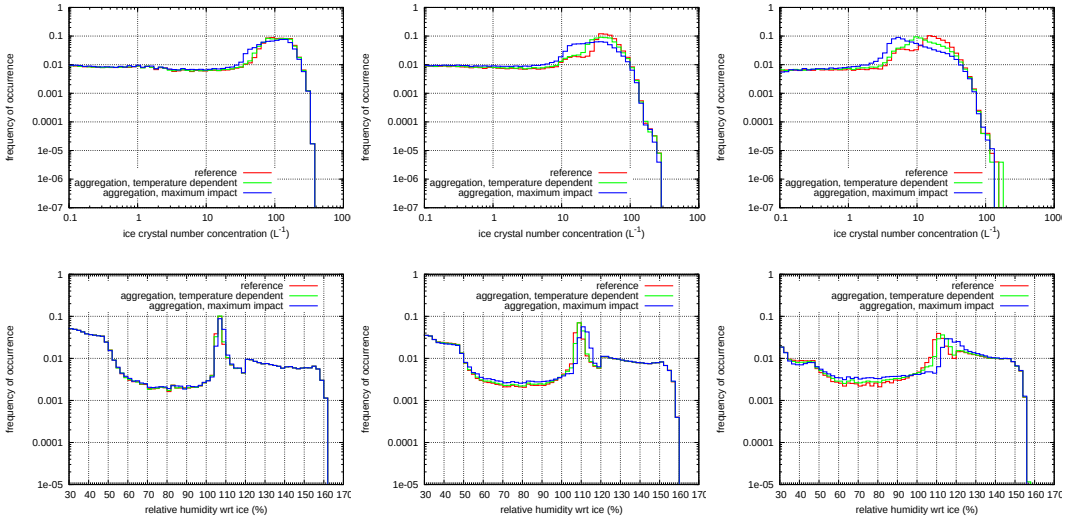

Fig. 10. Statistics of ice crystal number concentrations (top row) and relative humidity wrt ice (bottom row) for different temperature regimes (left: low temperature conditions, middle: medium temperature conditions, right: high temperature conditions).

ACPD
12, 23975–24009, 2012